DELPHI Collaboration

DELPHI 2000-005 PHYS 848
08 FEBRUARY 2000

VSAT Luminosity for the 1995 Scan

Ch. Zacharatou Jarlskog
Lund University

Abstract

The relative luminosity measurement performed by the Very Small Angle Tagger during the 1995 Z^0 scan is reported. The detector simulation, the systematic uncertainty and the comparison with the STIC luminosity are discussed.

1 Introduction

The luminosity monitors of e^+e^- storage rings benefit from the presence of Bhabha scattering, i.e. of the process[1] $e^+e^- \rightarrow e^+e^-$. At polar angles between 5 and 50 $mrad$, the scattering is in practice entirely described by a photon exchange in the t-channel. This ensures a low theoretical error on the calculation of the cross section. The lowest-order differential cross section can be approximated by the expression

$$\frac{d\sigma_0^{QED}}{dp_T} = \frac{2\pi\alpha^2}{p_T^3} \tag{1}$$

where p_T is the transverse momentum of the scattered particles. Eq. 1 implies a large forward peak, which gives to the process the additional advantage of high statistics.

The luminosity measurement in DELPHI is performed by two luminometers: the STIC detector, which calculates the absolute luminosity and the VSAT detector, whose task is to obtain a relative measurement with lower statistical error. This report presents the VSAT analysis with emphasis on the event selection and the dependence of the accepted cross section on variations of beam parameters.

2 Event selection and performance

The VSAT consists of four modules placed symmetrically to the DELPHI origin [1]. The modules in the forward region (C side) are called F1 and F2. The modules in the backward region are called B1 and B2. The modules F1 and B1 are located on the side of the beam pipe that is closest to the LEP center and are therefore labelled as inner modules in contrast with the modules F2 and B2, which are the so-called outer modules. One outer module together with the opposite inner module define one diagonal (arm) of the detector. We thus have two diagonals, named after the number of the forward module, i.e. diagonal one means F1-B2 and diagonal two means F2-B1. In either diagonal, the detector is triggered by coincidences with an energy deposit in each module greater than 20 GeV. These events are labelled as 'Bhabha triggers' and they form our initial sample. In order to extract the Bhabha set on which the luminosity calculation is performed, we first apply a set of cuts on an event-by-event basis, as described in the following subsections.

2.1 The energy measurement

We will first address the performance of the detector as far as the energy measurement is concerned, as this is of paramount importance for the event selection.

During the 1995 scan, the energy calibration was a complicated task because of the high contamination of our sample by events with wrongly assigned minibunch number[2]. Their majority consisted of high energy minibunch three data, representing approximately 10% of the total number of events. Their calibration is described in [2]. The rest of the

[1] The initial and final state radiation can be neglected for the purposes of this report.

[2] For the 1995 scan, LEP had modified its previous mode of single bunch operation to a scheme of tightly spaced minibunch-trains, i.e. instead of having only one bunch crossing every 25 μs there were 2 to 4 minibunches within each bunch. The time separation between minibunches was a fraction of a μs. Most of the scan data taking was done with 3 minibunches separated by about 250 ns.

mismatched events was a mixture of seven different combinations of minibunch numbers. They accounted for about 1% of the data. Their recovery is described in [3]. Moreover, the radiation accident of September 15 [4], having damaged the backward modules, entailed a separate treatment of the sample for the two periods before and after the accident. In spite of these complications, the energy calibration confirmed the stability of the modules: in fig. 1, we give the calibration constants for the four modules and the three minibunches. They have been extracted from the clean sample, after the mismatched events have been subtracted. The effect of the radiation accident is evident in the steps seen in the calibration constants of modules B2 and B1. The response of the modules was otherwise stable. The linearity of the modules is also established by fig. 1 as different fills have different beam energies.

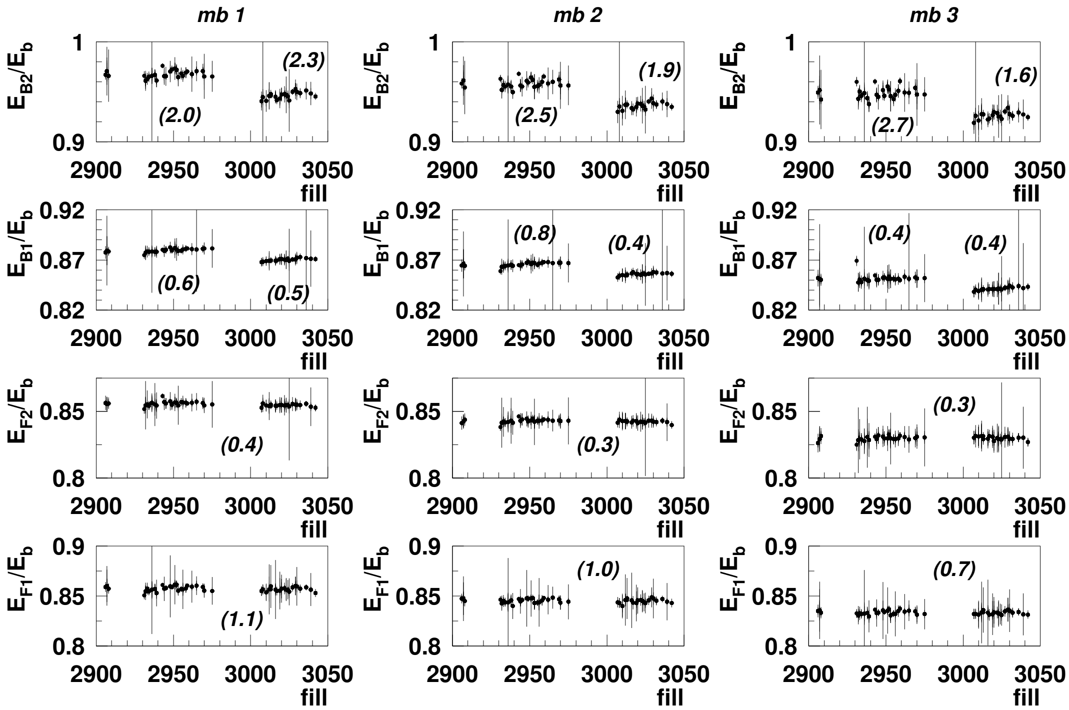

Figure 1: *Calibration constants for the four modules. The first, second and third column refer to events of minibunch one, two and three, respectively. The numbers in parentheses are the χ^2/dof for fits to constants. Two fits were done for each plot of modules B2 and B1 (corresponding to the periods before and after the radiation accident, i.e. before and after fill number 3000).*

2.2 Background subtraction

The background has two components: (a) accidental coincidences (also called false Bhabha events) and (b) coincidences between low energy depositions, mainly originating from off-momentum particles. The accidental coincidence rate is estimated by tagging one particle in one module and one particle in the diagonal module four beam crossings later. The low energy coincidences are removed from the data by applying a cut at 70% of the beam energy. However, there may be events where the particle's energy is above that cut but still lower than a full energy deposit. These refer to particles that have began to shower outside the module. Such particles have their maximum energy deposit in the inner x-strip of the detector and we thus use this x-position cut in order to remove them. An example of the above mentioned distributions for module B1, fill 3029, is given in fig. 2. There were 51221 triggers registered (solid line), 3190 (6%) of which were removed by the 70% energy cut on B1 (depicted by the arrow in fig. 2(a)). The same cut on the diagonal module discarded 3290 B1 events (dashed line). The accidental coincidences (dotted line) represented only 0.08% of the triggers (42 events). Fig. 2(b) shows that the x-position cut removed 2753 events (5%) (dashed line) and 3560 events (dotted line) of B1, i.e. 7% of the triggers, when applied on F2. The remaining Bhabha distribution contained 44268 events, i.e. 86% of the initial sample.

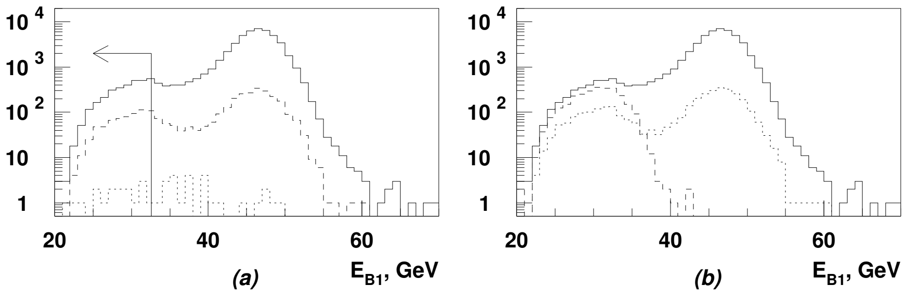

Figure 2: *The effect of background and position cuts on the Bhabha triggers of B1 (solid line): (a) energy cut on B1 (arrow) and on F2 (dashed line), accidental coincidences (dotted line), (b) x cut on B1 (dashed line) and on F2 (dotted line). (The vertical axes show numbers of events.)*

2.3 Acceptance cuts

The acceptance of the detector is restricted by the so-called radial cut. This cut defines a volume with outer edge corresponding to a maximum allowed radius of 7.7 cm (fig. 3(a)) and inner edge corresponding to a minimum allowed sum of the x positions ($sx = |x_{inner\ module}| + |x_{outer\ module}|$) equal to 13.2 cm (fig. 3(b)). The reason for the outer

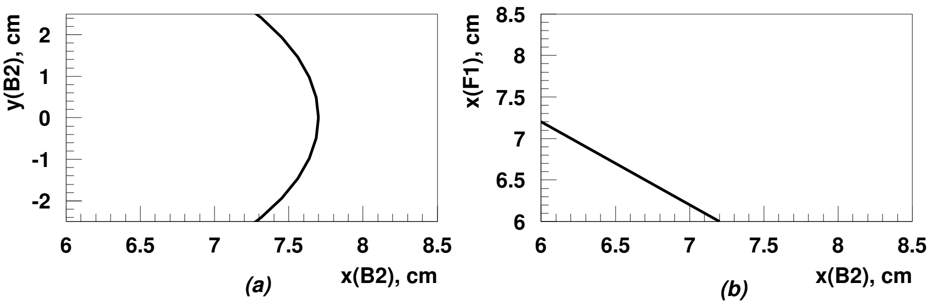

Figure 3: *The acceptance cuts; (a) the cut on the outer edge, (b) the cut on the inner edge of the detector.*

edge cut is the following. Upstream of the VSAT modules (at about 6.5 m from the interaction point), the x radius of the beam pipe is increased from 6 cm to 8 cm. In the connection region there is a thick flange which strongly absorbs the electrons with a large angle. From the (x, y) distribution of the impact points of the electrons in the VSAT we see that the absorption is not sharp and also that it is difficult to reproduce it faithfully with the simulation. For this reason, we set a cut at the value of the radius for which the (x, y) distributions of the data are compatible with the (x, y) distributions of the detector simulation FASTSIM (described in the following section). A similar argument holds for the cut at the inner edge. Again, by comparing the sx distributions of simulation and data, we see that there are small differences (of the order of few permille) at small sx. The events with very small sx are those in which both the forward and the backward electron have a small angle and thus a small x, that is they are both close to the inner edge of the VSAT module. These events are difficult to simulate faithfully because they depend critically on many parameters (beam position, beam tilt, etc.) and thus we set an sx cut at the value for which the sx distributions of the simulation and of the data are compatible.

The mean value of Bhabha events for the total volume (i.e. before applying the radial cut) was 3136 events per cassette in diagonal one and 3445 events per cassette in diagonal two. These numbers were reduced by 22% and 28%, respectively, when the acceptance cut was applied.

2.4 Corrupted data

Due to imperfections in the electronics, especially in the beginning of the run of 1995, the read out was occassionally corrupted. In order to remove the cassettes with high contamination we set two limits: first, the number of corrupted Bhabha triggers must be less than 10% and second, the number of corrupted buffers must be less than 1 permille. The reason for applying this cut is that we correct for the corrupted events that we miss using the trigger information which is generally available even if the buffer is corrupted, but this is a correction which has a large uncertainty, so it is valid only if the fraction of corrupted data is small, otherwise it introduces an error larger than the gain in statistics we would have by including the corrupted cassettes.

Fig. 4 shows the distributions of these two variables and the positions of the cuts. In order to decide on the values of the cuts we tried different combinations and we kept the one that gave the largest number of cassettes possible without allowing the normalized differences between STIC and VSAT luminosities to become too large. In total, the two cuts rejected 31% of the initial number of cassettes (1200).

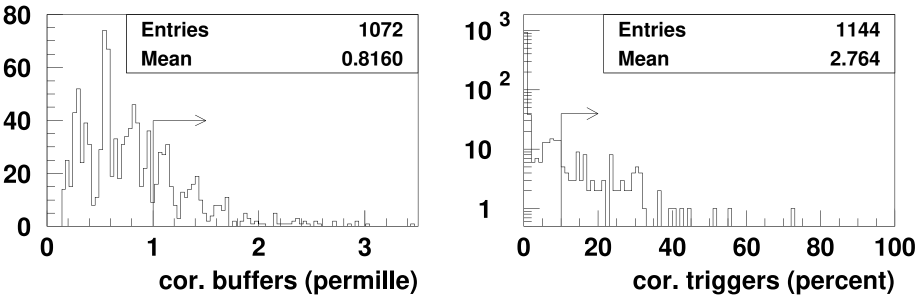

Figure 4: *Distributions of corrupted buffers and corrupted triggers. The arrows show the position of the cuts. The vertical axes show numbers of cassettes.*

3 The detector simulation

The visible Bhabha cross section can be evaluated by convoluting the theoretical cross section with the geometrical acceptance of the detector but as this task is very complicated the detector simulation is used instead. First, it determines the accepted cross section and then it calculates its dependence on beam parameter variations [5].

3.1 Description of FASTSIM

The events are generated with BHLUMI 4.03, where the radiative corrections are calculated with the YFS exponentiation, giving a theoretical uncertainty of 1.1 permille. Then FASTSIM tracks the particles from the interaction point to the detector dividing the path of the scattered particle into three transport regions [6]:

- from the interaction point to 3.7 m along the z-direction, i.e. through the magnetic field of the DELPHI solenoid,
- through the field of the superconducting quadrupoles, which are located between 3.7 m and 5.7 m along the beam axis and
- in the field-free region between the quadrupoles and the modules.

The motion of the particle through each of the above mentioned regions is represented by a matrix describing the transformation of the phase space coordinates. In order to reduce the execution time, the simulation ressorts to a number of approximations. First, the particles that hit the flanges or the material in front of them are discarded. Second, the beam pipe has to be taken into account: behind the flanges it is made of 1.5 mm of iron, which corresponds to 0.085 r.l., so it is possible that the outgoing particle's shower starts when it hits the beam pipe. FASTSIM calculates the thickness of the traversed material and adds it on the front of the module. The difference from the data is then that the angle between the shower products at the module's front face is not taken into account but this has no significant effect on the analysis. Particle synchrotron radiation in the magnetic fields is also neglected. Lastly, the longitudinal and transverse shower profiles are parametrized as described in [7].

3.2 The accepted cross section

After FASTSIM has calculated the energy and position of the particles that hit the detector, the events are analyzed by the same program we analyze the data with. The accepted cross section is then calculated as follows [8]. BHLUMI generates events according to the Born cross section and then modifies it by adding the radiative corrections. If σ_g is the (differential) Born cross section for a particular event and σ_i is the same cross section with all corrections, a weight $w_i = \sigma_i/\sigma_g$ is assigned to the event. After the event has passed the detector simulation and the experimental cuts we can calculate the average weight for all the accepted events $\overline{w} = \sum_{acc} w_i/N_{generated}$, where $N_{generated}$ is the number of generated events. The accepted cross section is then given by the expression $\sigma_{acc} = \overline{w} \cdot \sigma_{approx}$, where σ_{approx} is the integrated Born cross section for the kinematical region which was used for the run of BHLUMI.

3.3 Correction of the cross section for beam parameter variations

In order to correct the accepted cross section for the variation of the beam parameters, 29 FASTSIM runs were done. In 21 runs the x beamspot and the electron and positron divergences in x were varied. In the remaining 8 runs the electron and positron tilts in y were varied [8]. All runs had 1.2 million generated events, except for 9 of the 21 first runs, which had 2 million generated events.

In the simulation, the values of the x beamspot and divergence and of the y tilt were chosen so that the impact points of the electrons and positrons on the modules would be close to those of the real data. This is necessary because the corrections to be applied to the cross section are valid only for small variations of the average positions of the impact points, which have thus to be similar between real and simulated data. The average x and y positions of the simulated data are shown in fig. 5 for the two diagonals, compared with those of the real data: as one can see, the simulation is reasonably close to the real data, the small differences being tolerable within the statistical uncertainties of the correction factors (Table 1).

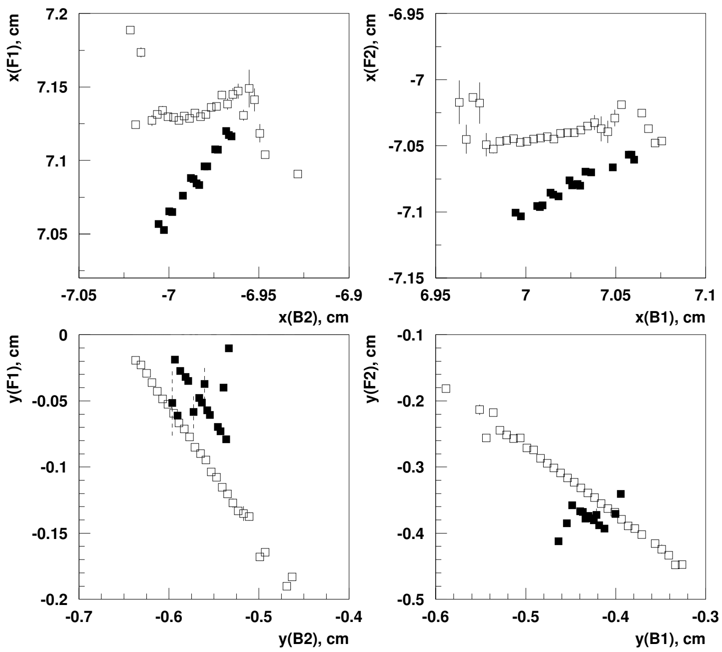

Figure 5: *Comparison between data (open squares) and FASTSIM (solid squares) for the coordinates of the impact points. (The positive tail values of the y(F1) distribution are not shown [7].)*

The correction of the cross section is subsequently done in terms of variables which are directly measured by the detector as follows [9]. For each FASTSIM run and for each diagonal i we calculate the accepted cross section σ_i and the variables Δx_i, $R\Delta x_i$, Δy_i and A_D defined as

$$\Delta x_i = x_i^{forward} + x_i^{backward}, \qquad \Delta y_i = y_i^{forward} + y_i^{backward}, \qquad A_D = \frac{N_1 - N_2}{N_1 + N_2}$$

where $x_i^{forward}$ ($x_i^{backward}$) is the x coordinate (averaged over the run) of the impact point of the particle on the forward (backward) module, $y_i^{forward}$ ($y_i^{backward}$) is the average y coordinate of the impact point of the particle on the forward (backward) module, N_1 (N_2) is the number of Bhabha events in diagonal one (two) and $R\Delta x_i$ is the dispersion of the Δx_i distribution. The corrected cross section of diagonal i is then

$$\sigma_i = \sigma_0[1-a_i(\Delta x_i-\overline{\Delta x_i})-b_i(\Delta x_i-\overline{\Delta x_i})^2-c_i(\Delta y_i-\overline{\Delta y_i})-d_i(R\Delta x_i-\overline{R\Delta x_i})-e_i(A_D-\overline{A_D})] \quad (2)$$

The mean values are those of the complete data sample. σ_0 is treated as an unknown constant. In order to calculate the coefficients (slopes) a_i, b_i, c_i, d_i, e_i we do fits to the corresponding distributions of σ_i, e.g. to calculate c_i we do a linear fit to the distribution of σ_i versus $\Delta y_i-\overline{\Delta y_i}$, etc. The results are given in Table 1. The small differences between diagonals one and two are due to small asymmetries in the setup.

	value for i=1	value for i=2
a_i (cm^{-1})	0.400 $\pm$ 0.030	-0.128 $\pm$ 0.020
b_i (cm^{-2})	1.800 $\pm$ 0.700	0.200 $\pm$ 0.500
c_i (cm^{-1})	-0.090 $\pm$ 0.030	-0.190 $\pm$ 0.030
d_i (cm^{-1})	0.300 $\pm$ 0.100	0.300 $\pm$ 0.100
e_i	0.001 $\pm$ 0.040	0.001 $\pm$ 0.040

Table 1: *Slopes for the 1995 scan.*

4 Results

4.1 Relative luminosity

According to eq. 2, the number of accepted Bhabha events in the data has to be corrected as follows

$$N^j = \frac{N_1^j}{1-a_1(\Delta x_1^j-\overline{\Delta x_1^j})+...}+\frac{N_2^j}{1-a_2(\Delta x_2^j-\overline{\Delta x_2^j})+...}$$

where N^j is the corrected number of events for the j-th cassette, N_i^j is the number of accepted Bhabha events in diagonal i and the denominators contain all the beam parameter corrections that we discussed in the previous section. We calculate the VSAT relative luminosity by adjusting the value of σ_0 so that the normalized differences with the STIC luminosity will be close to zero for the total data sample. The results are given in Table 2. The first four lines give the VSAT luminosity. Its values for all minibunch numbers, for minibunch one, two and three are given in lines one, two, three and four, respectively. The numbers referring to 'all' minibunches include also the Bhabha events that could not be associated with a specific minibunch number (unrecoverable mismatches), thus corresponding to the total Bhabha event sample. The next four lines give the corresponding values for STIC luminosity. Then the total numbers of VSAT and STIC Bhabha events are mentioned. In the next line of the table, we give the normalized differences (pulls) between VSAT and STIC luminosities for all minubunch numbers. We see that the pulls are acceptable. The errors for the VSAT luminosity follow, for all minibunches and for each minibunch separately. The total error is calculated by adding quadratically the statistical error and the systematic error. The systematic error stems mainly from the cross section correction for the beam parameters. For example, the correction for $R\Delta x_1$ is $d_1(R\Delta x_1 - \overline{R\Delta x_1})$, where d_1 is the slope, i.e. the correction factor given by FASTSIM, $R\Delta x_1$ is the value of the cassette currently processed and $\overline{R\Delta x_1}$ is the average value of $R\Delta x_1$ over all scan data. As a consequence, there are two contributions to the error, one due to the error of the slope, which comes from FASTSIM and is called correlated systematic error and the other being the error of $R\Delta x_1$ (depending on the statistics of the cassette) included in the uncorrelated systematic error. The uncorrelated error also includes the contribution of the uncertainties due to the energy and inner edge cut. The former is about 0.1 permille: it is due to the uncertainty of the trigger efficiency at the energies corresponding to the cut. The latter is estimated to be about 0.25 permille and it is due to the statistical error on the effect of the low sx

	mb	peak	peak-2	peak+2	total
L^{int}_{VSAT}	all	1752.54	4619.77	5520.35	11892.64
(nb^{-1})	1	580.63	1628.97	1951.87	4161.47
	2	619.18	1549.52	1870.15	4038.85
	3	550.50	1434.84	1691.23	3676.57
L^{int}_{STIC}	all	1736.78	4640.97	5515.72	11893.46
(nb^{-1})	1	571.33	1628.97	1948.72	4149.02
	2	614.71	1565.19	1873.14	4053.04
	3	550.21	1445.61	1692.03	3687.85
VSAT Bhabha events	all	612277	1681154	1859281	4152713
STIC Bhabha events	all	95232	266399	290134	651765
Pull	all	2.59	-2.15	0.41	-0.05
VSAT stat. error	all	1.28	0.77	0.73	0.49
(permille)	1	2.22	1.30	1.23	0.83
	2	2.15	1.33	1.26	0.84
	3	2.28	1.38	1.33	0.88
VSAT unc. syst. error	all	0.28	0.17	0.16	0.11
(permille)	1	0.50	0.29	0.28	0.18
	2	0.48	0.29	0.28	0.19
	3	0.51	0.31	0.30	0.20
VSAT cor. syst. error	all	0.34	0.42	0.37	0.09
(permille)	1	0.41	0.52	0.26	0.22
	2	0.33	0.41	0.49	0.19
	3	0.36	0.43	0.47	0.11
VSAT tot. syst. error	all	0.44	0.45	0.41	0.14
(permille)	1	0.64	0.59	0.38	0.29
	2	0.58	0.50	0.56	0.26
	3	0.62	0.53	0.56	0.22
VSAT total error	all	1.35	0.89	0.84	0.51
(permille)	1	2.31	1.43	1.29	0.88
	2	2.23	1.42	1.38	0.88
	3	2.36	1.48	1.44	0.91
STIC error (permille)	all	3.24	1.94	1.85	1.24

Table 2: *STIC and VSAT luminosities.*

cut in real and simulated data. We also state the STIC error for comparison. The total VSAT error is significantly better than the STIC error. The values of the third, fourth and fifth column represent data taken at 45.66 GeV (peak), 44.74 GeV (peak-2) and 46.51 GeV (peak+2), respectively. The quantities in the last column refer to all energies.

4.2 Comparison with STIC

The main use of the VSAT measurement was to cross check the results of STIC. First, a comparison was made of the percentage of events registered in each minibunch (fig. 6). The measurements agree within the errors, of the order 0.1 %.

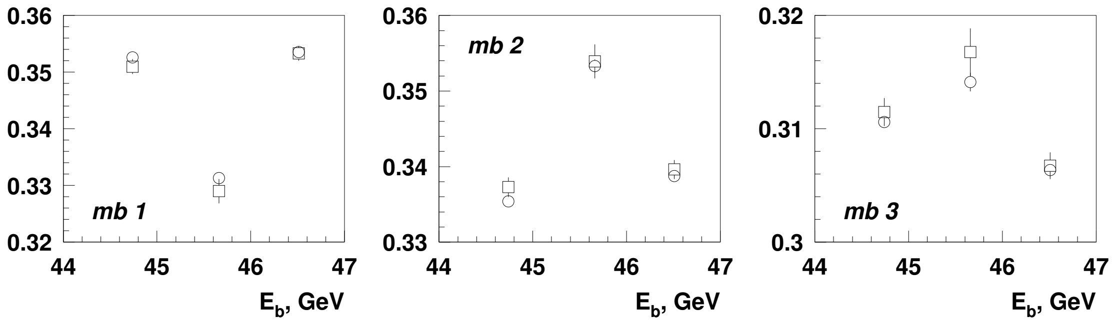

Figure 6: *Number of events in the three minubunches divided by the total number of events for the three nominal energies. The STIC data are shown by the squares and the VSAT data by the circles .*

The luminosity agreement can be confirmed by calculating the normalized differences at the three energy points and for the three minibunches separately. The results are given in fig. 7. The rms is close to unity for all distributions. We conclude that the two measurements have followed each other, as can also be seen in the correlation plots of fig. 8.

5 Conclusions

Due to reduced statistics, mainly at the peak position, the contribution of the VSAT result to the 1995 scan luminosity is only a marginal improvement. The result is consistent with that of STIC and with smaller errors thus reliably cross checking the latter measurement.

Acknowledgements

I wish to express my deepest gratitude to my supervisor G. Rinaudo for her invaluable guidance and support during this analysis. I would also like to thank S. Almehed for producing the simulated data and answering many questions throughout my work with the VSAT.

References

[1] Almehed et al., *A silicon tungsten electromagnetic calorimeter for LEP*, Nucl. Instr. Meth. A305 1991.

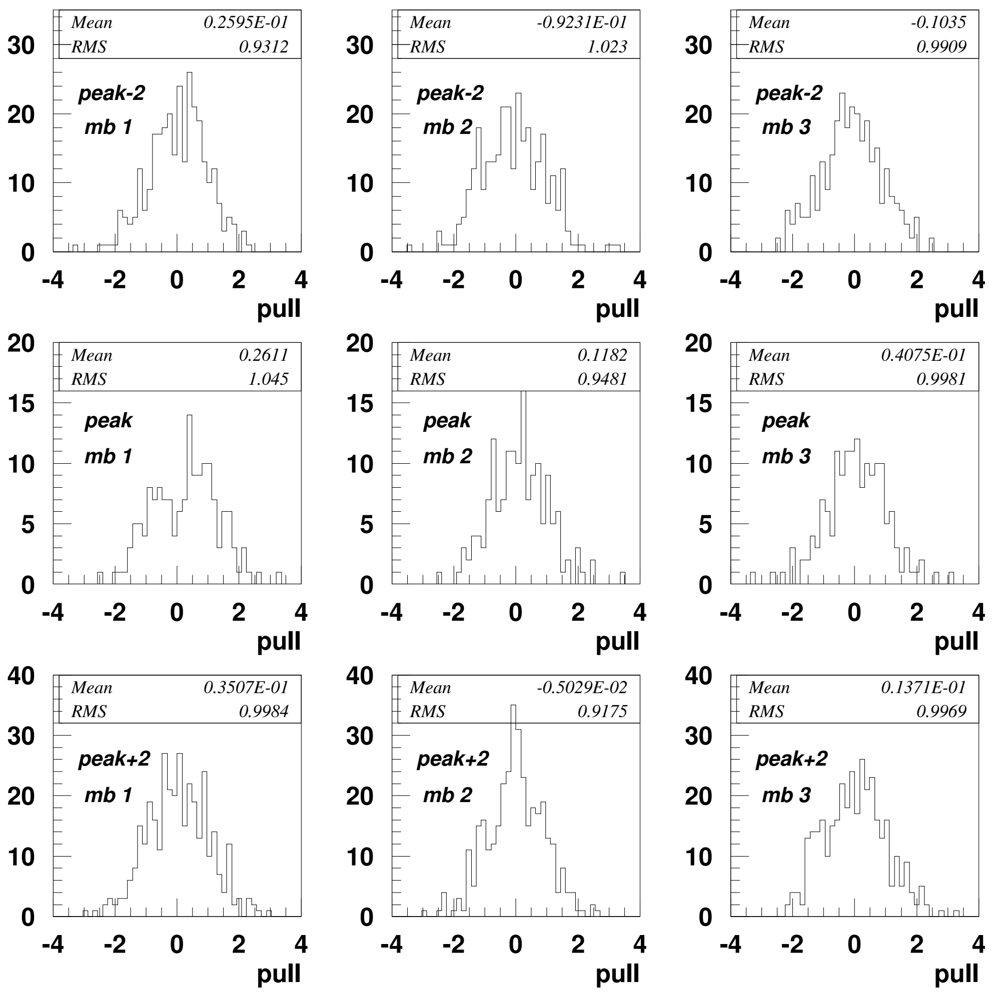

Figure 7: *Normalized differences for STIC and VSAT luminosities at the three beam energies and for the three minibunches.*

[2] Ch. Jarlskog, *VSAT energy calibration for 1995 minibunch data*, LUNFD6/(NFFL-7129) 1996.

[3] Ch. Jarlskog, *VSAT Off-line Minibunch Tagging for the 1995 Scan*, LUNFD6/(NFFL-7154) 1998.

[4] I. Kronkvist, *Data Base and Slow Controls System of the DELPHI VSAT and Two-Photon Physics using DELPHI at LEP*, PhD thesis, LUNFD6/(NFFL-7128) 1996.

[5] Ch. Jarlskog, G. Rinaudo, *Measurement of the beam parameters during the 1995 Z^0 scan with the DELPHI VSAT*, DELPHI note in preparation.

[6] A. Håkanson, *Luminosity Measurement at LEP using the Very Small Angle Tagger of DELPHI*, PhD thesis, LUNFD6/(NFFL-7077) 1993.

[7] Ch. Jarlskog, *Luminosity Measurement for the 1995 Z^0 scan with the Very Small Angle Tagger of DELPHI*, licentiate thesis, LUNFD6/(NFFL-7160) 1998.

[8] S. Almehed, private communication.

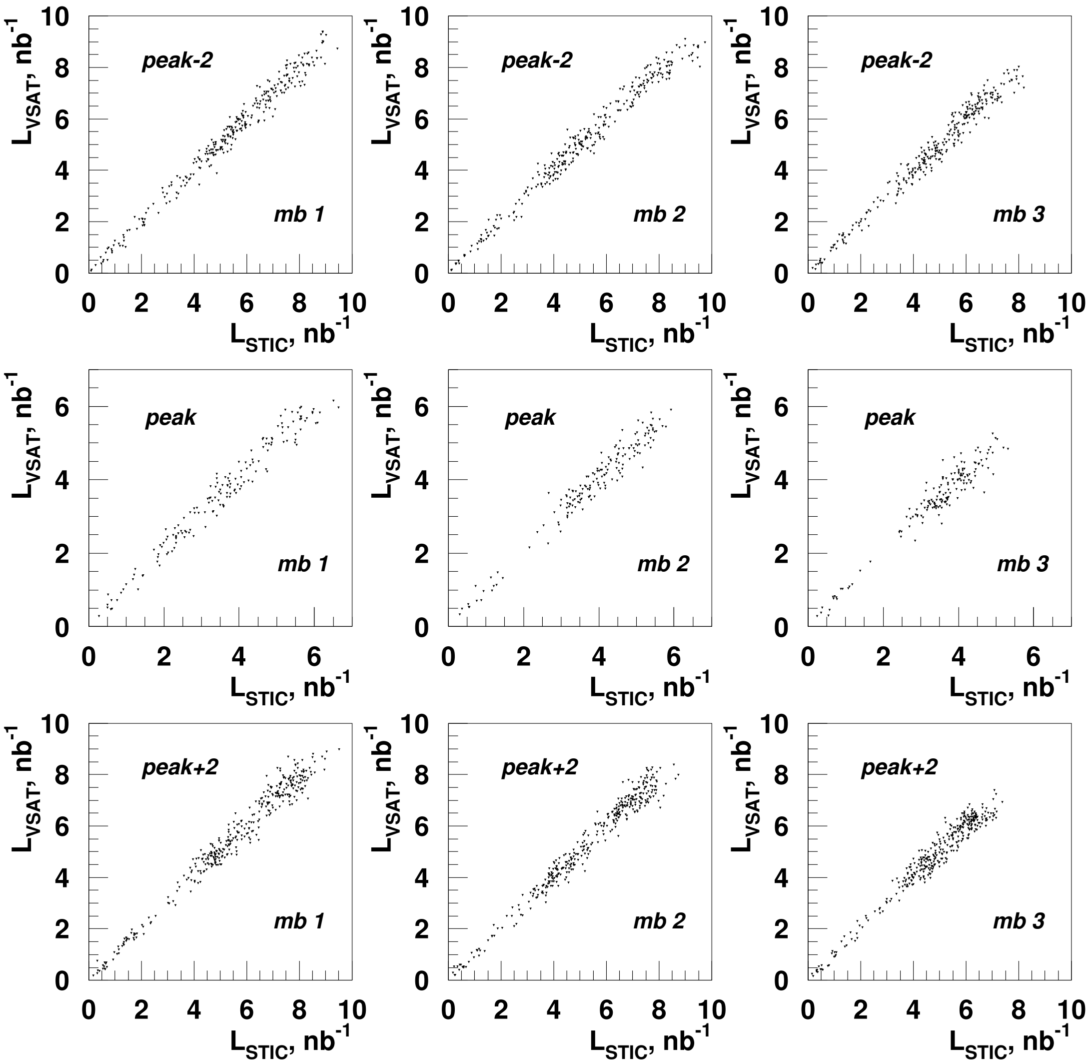

Figure 8: *Luminosity correlation plots at the three beam energies and for the three mini-bunches.*

[9] G. Rinaudo, private communication.